

Fingering instability and mixing of a blob in porous media

Satyajit Pramanik* and Manoranjan Mishra

Department of Mathematics, Indian Institute of Technology Ropar, Rupnagar 140001, India

(Received 5 April 2016; published 11 October 2016)

The curvature of the unstable part of the miscible interface between a circular blob and the ambient fluid in two-dimensional homogeneous porous media depends on the viscosity of the fluids. The influence of the interface curvature on the fingering instability and mixing of a miscible blob within a rectilinear displacement is investigated numerically. The fluid velocity in porous media is governed by Darcy's law, coupled with a convection-diffusion equation that determines the evolution of the solute concentration controlling the viscosity of the fluids. Numerical simulations are performed using a Fourier pseudospectral method to determine the dynamics of a miscible blob (circular or square). It is shown that for a less viscous circular blob, there exist three different instability regions without any finite R -window for viscous fingering, unlike the case of a more viscous circular blob. Critical blob radius for the onset of instability is smaller for a less viscous blob as compared to its more viscous counterpart. Fingering enhances spreading and mixing of miscible fluids. Hence a less viscous blob mixes with the ambient fluid quicker than the more viscous one. Furthermore, we show that mixing increases with the viscosity contrast for a less viscous blob, while for a more viscous one mixing depends nonmonotonically on the viscosity contrast. For a more viscous blob mixing depends nonmonotonically on the dispersion anisotropy, while it decreases monotonically with the anisotropic dispersion coefficient for a less viscous blob. We also show that the dynamics of a more viscous square blob is qualitatively similar to that of a circular one, except the existence of the lump-shaped instability region in the R - Pe plane. We have shown that the Rayleigh-Taylor instability in a circular blob (heavier or lighter than the ambient fluid) is independent of the interface curvature.

DOI: [10.1103/PhysRevE.94.043106](https://doi.org/10.1103/PhysRevE.94.043106)

I. INTRODUCTION

Fluid flow and mixing in porous media [1,2] are active areas of research devoted to characterize industrial and environmental processes, such as oil recovery [3], pollution remediation [4], carbon dioxide sequestration [5–7], and chromatography separation [8–10], to name a few. Fluid flow in porous media can feature hydrodynamic instabilities, such as viscous fingering (VF) or Saffman-Taylor instability [3] and Rayleigh-Taylor instability [11], depending on the flow configuration and physical properties of the fluids. VF is observed when a less viscous and hence a more mobile fluid displaces a more viscous one in porous media [3,12–15]. On the other hand, a convective instability is featured when a heavier fluid is placed above a lighter one with the gravity aligned vertically downwards [11,16]. In both the cases the interface deforms into “fingers,” which enhances mixing between the two fluids. The buoyancy-induced convective instability is also known as density fingering (DF), as the density gradient is the driving force in this case. A large body of literature is devoted to the understanding of VF and/or DF at a single planar interface between two nonreactive [11,14,15,17–19] and reactive fluids [16,20]. In liquid chromatography column, the sample confined in a finite rectangular region [8] can feature VF instability at the frontal or rear planar interface depending on the viscosity contrast between the sample and the displacing fluid [18]. However, in numerous cases, for instance, in localized contaminant [4], CO₂ plumes dissolved in brine or oil, the localized fluids of different viscosity and/or

density from the ambient fluid may not necessarily feature planar interface [21]. In the case of pollutant contamination in soil, the viscous or buoyant spills can be of an arbitrary initial shape, which is drifted by groundwater flows. Similarly, in CO₂ sequestration, an irregular plume of the injected supercritical CO₂ sample migrates within the subsurface water or brine of different physical properties, such as viscosity or density [5–7].

In addition to arbitrary initial geometrical shape of the sample, the viscosity and density of the finite sample can also vary in a wide range depending on its composition. The ambient fluid can be more viscous than the contaminant, e.g., trichloroethane, methylene chloride, dichloroethylene, chloroform, gasoline, alcohols, and methyl tertiary butyl ether, or it can be less viscous, e.g., ethylene dibromide, dibutyl phthalate, *m*-cresol, jet fuel, CO₂ dissolved brine, etc. [5,21,22]. Mixing plays an important role in many natural and industrial processes, such as food processing [23], mantle convection [24], bacterial locomotion [25,26], groundwater flows in heterogeneous media [27], and chemical reaction [2,27], to name a few. VF enhances mixing of fluids in porous media or in microfluidics at low Reynolds number [1]. Jha *et al.* [2] coupled VF with alternating injection of a finite slug of sample and the ambient fluid to effectively increase the mixing in porous media.

Despite having enormous importance, understanding the flow around a sample of arbitrary shape and viscosity or density remains poorly explored. VF in a miscible blob was investigated both numerically [20,28] and experimentally [29]. De Wit *et al.* [20] reported that when a less viscous miscible blob is very small, an ellipse deformation and no fingering are observed. Chen *et al.* [28] explored the influence of velocity divergence and the Korteweg stress on the dynamics of a less viscous miscible circular blob through numerical simulations of Darcy's law for flow in a homogeneous porous medium. It

*Present address: Nordic Institute for Theoretical Physics (NORDITA), SE-10691, Stockholm, Sweden; satyajit.math16@gmail.com

was shown that the Korteweg stress helps in formation of an upstream tail and stabilizes VF at the leading part of the circular blob with an unfavorable viscosity contrast [28]. Dispersion and miscible VF of initially circular more viscous blob within a rectilinear displacement were analyzed experimentally by Maes *et al.* [29]. VF formed at the concave interface of the circular blob due to an unstable viscosity contrast between the circular blob and the ambient fluid, while the convex interface develops a downstream tail [29]. Nicolaides *et al.* [21] investigated the impact of VF and permeability heterogeneity on breakthrough and clean-up times, mixing, and dilution of a contaminant migrating through an aquifer. They showed that the viscosity contrast between the contaminant and the ambient fluid plays an important role in mixing efficiency and groundwater clean up [21]. For buoyancy-driven fingering, Mainhagu *et al.* [30] have investigated experimentally the behavior of a dense contaminant injected from a point source in a fracture. Recently, Sajjadi and Azaiez [31] discussed heat and mass transfer in melting porous media in the framework of stable miscible displacements. They discussed the tendency for the flow to circumvent a frozen square or rectangular block. The fluid flow problem of their study is similar to the flow past a miscible blob.

Discussion of the above literature reveals that understanding of fluid mixing in rectilinear displacement of a miscible sample of arbitrary geometrical shape having different physical properties than the carrier fluid requires more attention. We ask the following practical question: How does the viscosity or density gradient determine the spatial structure and temporal evolution of the miscible blob that characterizes spreading, mixing, and dilution of the plume in the ambient fluid? This question has been answered by numerically integrating a convection-diffusion equation for the solute concentration ruling the dynamic viscosity and density of the fluids coupled to Darcy's law for the fluid velocity. Numerical simulations are performed using a Fourier pseudospectral method [8,15] for a wide range of parameter values, such as log-mobility ratio R , Péclet number Pe , and the initial area A_0 of the blob. When a less viscous circular blob is sufficiently large, VF is observed at the frontal interface for all values of R and Pe scanned. On the other hand, for a more viscous blob, only a finite window of R features VF at the rear interface above a critical value of Pe and A_0 . It is observed that the critical values of Pe and A_0 for a more and less viscous blob differ. We characterize quantitatively the mixing, spreading, and dilution of the blob in different instability regions by measuring the variances of the sample in time. Contrary to VF, for buoyancy-driven convection, the spatial structure and temporal evolution of the fingers at the interface with unstable density gradient are identical for both heavier and lighter blobs. Our results pave the way to the understanding of mixing of plumes of arbitrary shape and physical properties in porous media.

This paper is organized as follows. The problem description and mathematical formulation is described in Sec. II. This section also describes the method of numerical solution. The numerical results obtained are discussed in the subsequent sections. The dynamics of a more (circular as well as square) and less (circular) viscous miscible blob is discussed in Sec. III. This is followed by a parametric study of various qualitative and quantitative properties of the flow in Sec. IV. Section V

discusses the density fingering of a heavy as well as a light miscible circular blob. The concluding remarks and the future perspectives are mentioned in Sec. VI.

II. MATHEMATICAL FORMULATION AND NUMERICAL SOLUTION

The mathematical formulation of the physical problem, dimensionless formulation, and the numerical method of solution of the problem are discussed in the following subsections.

A. Physical description of the displacement flow

Consider a rectilinear displacement of a circular blob consists of some solute dissolved in a solvent in two-dimensional homogeneous porous media initially filled with the same solvent (see Fig. 1 for the schematic of the displacement flow). The fluids are viscous, neutrally buoyant, incompressible, nonreactive, and miscible with each other. Dynamic viscosity of the ambient fluid and the blob are μ_1 and μ_2 , respectively. The initial radius of the blob is denoted by r_d , solute concentration inside the blob is $c = c_2$, and $c = 0$ outside the blob. The ambient fluid is injected at a uniform velocity $U\hat{i}$ from left to right, where \hat{i} is the unit vector along the x axis. The viscosity of the fluids depends on the solute concentration c . The dimensional length and width of the domain is L and W , respectively.

B. Governing equations and dimensionless formulation

The fluid incompressibility is represented by the divergence-free velocity, which satisfies Darcy's law. The solute concentration follows a convection-diffusion equation. Following Pramanik *et al.* [32], for the dimensionless formulation, we use $V_c = U$, $L_c = W/16$, $\tau_c = L_c/V_c$, $\mu_1 V_c L_c/\kappa$, μ_1 , and c_2 as the characteristic velocity, length, time, pressure, viscosity, and concentration, respectively. Here, κ is the permeability of the porous media. The dispersion is taken to be anisotropic having D_x and D_y as the axial and the transverse dispersion coefficients, respectively. The related dimensionless equations in a reference frame moving with the (dimensional) velocity U are [32,33]

$$\nabla \cdot \underline{u} = 0, \quad (1)$$

$$\nabla p = -\mu(c)(\underline{u} + \hat{i}), \quad (2)$$

$$\frac{\partial c}{\partial t} + \underline{u} \cdot \nabla c = \frac{1}{Pe} \left(\frac{\partial^2 c}{\partial x^2} + \epsilon \frac{\partial^2 c}{\partial y^2} \right), \quad (3)$$

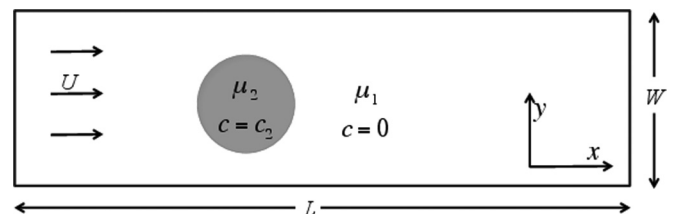


FIG. 1. Schematic of the displacement of circular blob in two-dimensional homogeneous porous media.

where $\underline{u} = (u, v)$ is the two-dimensional Darcy velocity and $\mu(c) = e^{Rc}$ [3]. The dimensionless initial radius $r = r_d/L_c$, the Péclet number $Pe = UL_c/D_x$, the anisotropic dispersion coefficient $\epsilon = D_y/D_x$, and the log-mobility ratio $R = \ln(\mu_2/\mu_1)$ are the four dimensionless parameters of the problem.

C. Initial and boundary conditions

Description of appropriate initial and boundary conditions makes the mathematical formulation of the above problem complete. We use doubly periodic boundary conditions both for the fluid velocity and the solute concentration, i.e.,

$$(\underline{u}, c)(0, y, t) = (\underline{u}, c)(L_x, y, t), \tag{4}$$

$$(\underline{u}, c)(x, 0, t) = (\underline{u}, c)(x, L_y, t), \tag{5}$$

along the longitudinal and transverse directions, respectively. Here L_x and L_y correspond to the dimensionless length and width of the computational domain.

The initial condition for the solute concentration is given as

$$c(x, y, t = 0) = \begin{cases} 1, & \text{inside the blob} \\ 0, & \text{outside the blob.} \end{cases} \tag{6}$$

Although, the velocity does not have any explicit time derivative in Eqs. (1)–(3), an initial condition for velocity \underline{u} is required to solve the convection-diffusion equation (3). An appropriate initial condition for the velocity in the moving reference frame is

$$\underline{u}(x, y, t = 0) = (0, 0). \tag{7}$$

D. Method of solution

The stream function, $\psi(x, y, t)$ (such that $u = \frac{\partial \psi}{\partial y}$ and $v = -\frac{\partial \psi}{\partial x}$), form of the governing equations becomes [33]

$$\nabla^2 \psi = -R \nabla c \cdot (\nabla \psi + \underline{j}), \tag{8}$$

$$\frac{\partial c}{\partial t} + \frac{\partial \psi}{\partial y} \frac{\partial c}{\partial x} - \frac{\partial \psi}{\partial x} \frac{\partial c}{\partial y} = \frac{1}{Pe} \left(\frac{\partial^2 c}{\partial x^2} + \epsilon \frac{\partial^2 c}{\partial y^2} \right), \tag{9}$$

where \underline{j} is the unit vector in the y direction. These equations are numerically solved using a Fourier pseudospectral method initially employed by Tan and Homsy [15] and later successfully used by many researchers in the studies of miscible viscous and density fingering problems [8,10,11,17,18,32]. In order to ensure that the dynamics of the blob remains unaffected by the influence of the periodic boundaries, the initial radius of the blob considered in this paper satisfies $L_y/r \geq 32$, and $L_x/r \geq 64$, i.e., the blob is situated away from the boundaries. The number of spectral nodes chosen for a computational domain of size 32×16 is 4096×2048 . The step size of the spatial discretization, $\Delta x = \Delta y = 1/2^7$, is sufficiently small to capture the resolution of the interface of the circular blob. Various panels in Figs. 2–8 show only a small fraction of the numerical domain. Unlike the cases of VF around planar interfaces, no initial perturbations are required at the diffusive interface between the blob and the displacing fluid to trigger the instability, as curvature naturally ensures instability via Eqs. (8), due to the fact that ∇c and $\nabla \psi$ are not collinear at the curved miscible interface [32]. The time step used is $\Delta t = 10^{-4}$. A convergence study of the numerical method ensures that the fingering dynamics is not affected when using smaller time and spatial discretizations. The accuracy and efficiency of the Fourier pseudospectral method has been verified by calculating the total mass of the blob, which shows a maximum 0.001% relative error. The

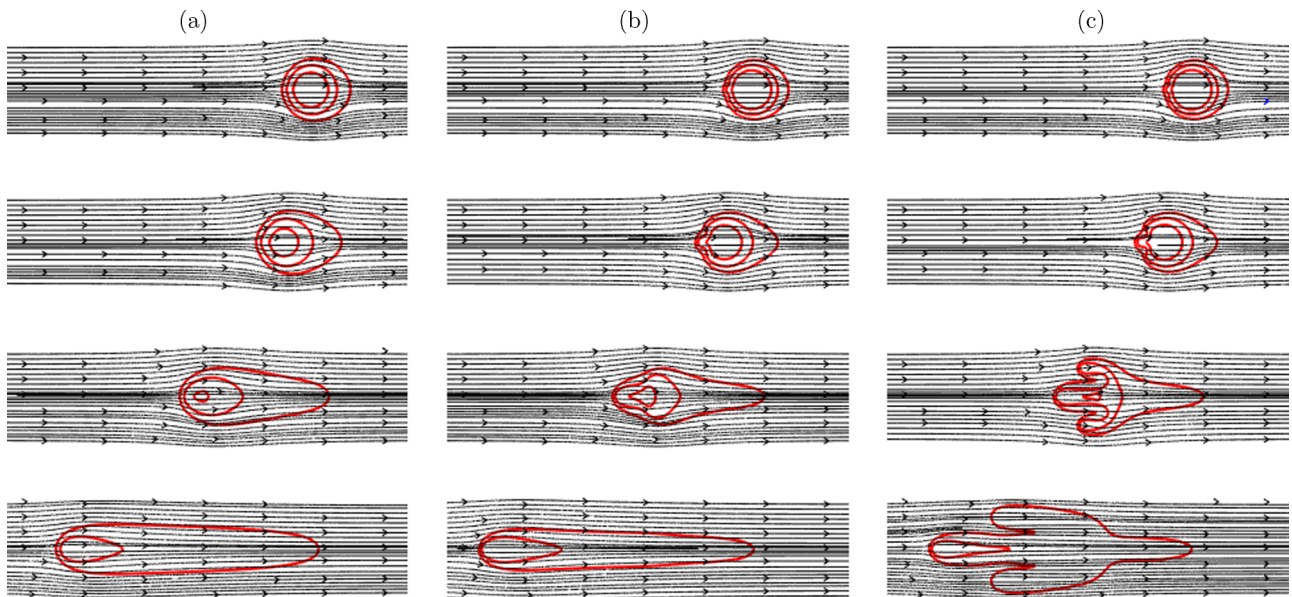


FIG. 2. Streamline distribution in the vicinity of the circular blob of initial radius $r = 0.5$ at time $t = 1, 2, 5, 10$ (from top to bottom) for $R = 1.25$: (a) $Pe = 500$, (b) $Pe = 900$, and (c) $Pe = 1000$. The red contours correspond to $c = 0.01, 0.50, 0.99$ (from outside to inside).

pseudospectral method leads to numerical instability for large values of Pe and R [1,15,33]. Therefore, in this paper, we restrict our numerical experiments for the parameter ranges, $|R| \leq 2.5$, and $Pe \leq 1500$.

III. DYNAMICS OF A MORE OR LESS VISCOUS BLOB

In a recent paper, Pramanik *et al.* [32] investigated viscous fingering and deformation of a more viscous miscible circular blob in a rectilinear displacement in homogeneous porous media. Pramanik *et al.* [32] showed that three different instability modes (viscous fingering and comet- and lump-shaped deformation) can appear depending on the size of the blob, log-mobility ratio, and Péclet number. Furthermore, they mentioned the existence of a finite R window for VF of a more viscous circular blob above a critical radius and the critical Péclet number. The main focus of this paper is to understand the dynamics of a less viscous circular blob in the rectilinear displacement and compare with the corresponding more viscous blob [32] under the same flow conditions. What follows is, in essence, a brief summary of the results of the R - Pe parameter space for a more viscous circular blob [32] with some additional information. This is followed by the discussion of the dynamics of a more viscous square blob. Finally, we discuss in detail the dynamics of a less viscous circular blob and compare with the corresponding more viscous blob, wherever applicable. In this section, we confine our focus to the case of isotropic solute dispersion, $\epsilon = 1$.

A. Dynamics of a more viscous circular blob

The nature of deformation and instability depends on various flow parameters. For a given $r = 0.5, \epsilon = 1$, Pramanik *et al.* [32] summarizes the stability characteristics in R - Pe parameter space, which is divided into three instability regions: VF and lump- and comet-shaped deformations. The observed dynamics corresponding to each point in this parameter space is a combined effect of R and Pe . Variation from one type of instability to other while moving along a particular path crossing the boundaries is associated with particular physical consequence. The individual effect of R on the fingering instability and the deformation of the blob has been discussed for a fixed Pe ($> Pe_c$) by Pramanik *et al.* [32]. For a given Pe , different R values are associated with different relative velocities between the blob and the ambient fluid, which results in different instabilities. A natural question follows: Why does the length of the tail increases with R ? The Darcy velocity is directly proportional to the pressure gradient, and the proportionality constant, the dynamic viscosity of the fluid, varies locally depending on the concentration, c . Thus, for a given ∇p , the variation of the Darcy velocity in the vicinity of the blob depends on the space-time evolution of c . For

$$\mu(c) = e^{Rc}, \quad R > 0, \quad (10)$$

the dynamic viscosity decreases as c decreases. Thus, the mobility of the fluid increases away from the center of the blob. The ambient fluid sweeps away the diffused layer in the downstream direction, which results in formation of downstream tail. From the viscosity-concentration relation (10) it is evident that the mobility variation in the vicinity

of the blob increases rapidly as R increases. Therefore, the velocity of the comet head relative to its tail increases with R , which results in a longer tail for a larger log-mobility ratio. This is readily evident from the streamline distribution inside the tail (not shown here for brevity).

One can study the individual effect of Pe [i.e., effect of diffusion (injection velocity), provided that the injection velocity (diffusion) remains unchanged] by moving along the lines of constant R in the R - Pe parameter space. The spatial structure and temporal evolution of the blob corresponding to three sets of parameters along the vertical line $R = R_c$ in the phase space (see Fig. 4 of Pramanik *et al.* [32]) are presented in Fig. 2. To investigate the effect of different Pe , we recall that the initial viscosity contrast between the blob and the ambient fluid are the same for all three cases. We assume that the displacement velocity remains the same for all three cases. Therefore, one can explain that diffusion of the solute concentration is responsible for the different instability modes that are observed when Pe crosses two critical values. The first one corresponds to the transition from comet- to lump-shaped instability, while the second one represents the critical value for the onset of VF. When the diffusion is faster ($Pe \lesssim 750$), the destabilizing viscosity contrast is dominated by the stabilizing action of diffusion. This deforms the blob into a comet shape having a short and blunt tail in the downstream direction. When the diffusion is relatively slower ($Pe \gtrsim 925$), the viscosity contrast becomes dominant, which results in VF at the trailing interface [see Fig. 2(c)]. For intermediate values of Pe , i.e., $750 \lesssim Pe \lesssim 925$, the viscous and the diffusive forces compete with each other, resulting a lump-shaped instability to the circular blob [see Fig. 2(b)].

The discussion of this subsection (Sec. III A) helps the readers to understand and relate the results of the remainder of the paper. The discussed physical effects of this section, associated with R and Pe , are referred to in the subsequent discussion.

B. Dynamics of a more viscous square blob

In Sec. III A we have discussed how a more viscous miscible circular blob features three distinct instability modes depending on R and Pe . How do these instability modes alter in the R - Pe parameter space for an initially square blob? We choose a square blob of diagonal length $2r$ having its sides parallel to the coordinate axes. With this choice, the square blob can be inscribed inside a circle of radius r [see Fig. 3(a) for the schematic of the flow].

It is observed that the displacement of a more viscous square blob and a more viscous circular blob possesses certain dynamic similarities. For instance, VF is observed over a finite R window when $Pe > Pe_c$. However, unlike the case of a circular blob, the R - Pe parameter space for a square blob features only VF and comet-shaped instabilities. The intermediate region of lump-shaped instability disappears in the case of square blob. Figure 3(b) shows different instability regions in R - Pe plane for a square blob with $R > 0$ and $r = 0.5$. This shows that the VF region increases significantly for a square blob compared to the circular one. A careful observation of the parameter space corresponding to both the circular blob (see Fig. 4 in Pramanik *et al.* [32]) and the square blob [Fig. 3(b)] reveals that the region II (VF) in the latter

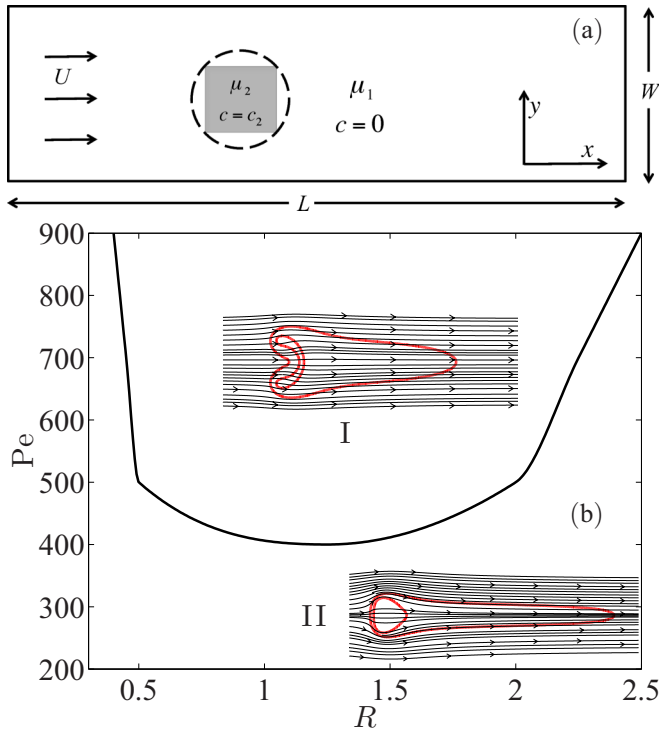


FIG. 3. (a) Schematic of the displacement of an initially squared miscible blob in a homogeneous porous medium. (b) Phase plot in R - Pe plane for $r = 0.5$ shows two distinct instability regions: VF (I) and comet-shaped deformation (II). Streamlines in the vicinity of the blob (red contour lines) are presented for $Pe = 500$, $R = 1.25$ (I), and $Pe = 900$, $R = 2.5$ (II).

case contains both the regions II and III (VF and lump-shaped instability) of the former. The critical Péclet number, Pe_c , for the onset of VF in the former case is much smaller than that in the latter. In particular, for $r = 0.5$, $Pe_c \approx 925$ for a circular blob and for a square blob $Pe_c \approx 400$.

The spatiotemporal distributions of the solute concentration of an initially squared blob are shown in Fig. 4 at different

dimensionless times. The diagonal length of the square blob is taken to be 1. To discuss the influence of Pe (i.e., diffusion or injection velocity) and viscosity contrast on the observed dynamics of viscous fingering and comet-shaped deformation, we choose the following three parameter sets from the R - Pe parameter plane: (a) $R = 1.25, Pe = 300$, (b) $R = 1.25, Pe = 900$, and (c) $R = 2.5, Pe = 900$ (see Fig. 4). The physical justification of the observed dynamics is similar to that discussed in Sec. III A. The influence of Pe can be analyzed from Figs. 4(a) and 4(b) corresponding to the first two parameter sets. These figures confirm the existence of a critical Péclet number, Pe_c , for the onset of VF as shown in Fig. 3. On the other hand, the influence of the viscosity contrast on the spatiotemporal dynamics of the blob is understood by analyzing Figs. 4(b) and 4(c), which correspond to the parameter sets (b) and (c). This figure pair confirms the finite R window for VF in a square blob. In summary, the dynamics of a more viscous finite blob of different initial shape (e.g., circular or square) has certain qualitative features in common. It will be interesting to explore further for miscible blob of other initial shape, in particular, of an arbitrary shape.

C. Dynamics of a less viscous circular blob

Consider the displacement of an initially circular blob, which is less viscous than the surrounding fluid ($R < 0$). This type of viscosity contrast is relevant to the dynamics of a localized zone of CO_2 saturated brine displaced by pure brine [5], although the actual CO_2 sequestration problem possesses different physical conditions. Other fluid pairs, in the form of different contaminant in aquifer water, are also listed in Sec. I. We are interested in knowing whether the dynamics of a less viscous circular blob is identical to that of a more viscous one [32] under the identical flow conditions. In order to compare the dynamical behaviors between these two cases, the spatiotemporal evolution of the concentration is presented in Fig. 5 for $r = 0.5$, $Pe = 1000$, and $R = -0.5, -1.0$, and -1.5 . This figure shows that instability becomes stronger and the blob mixes quickly into the ambient fluid as the magnitude of

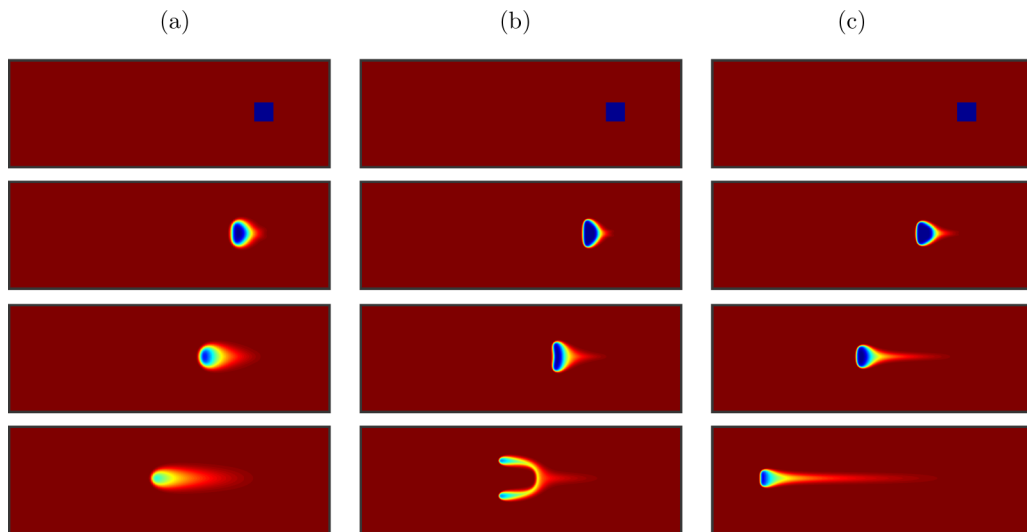


FIG. 4. Spatial distribution of concentration in the moving frame of reference at times $t = 0, 2, 5, 10$ from top to bottom for $r = 0.5$, $(Pe, R) =$ (a) $(300, 1.25)$, (b) $(900, 1.25)$, and (c) $(900, 2.5)$.

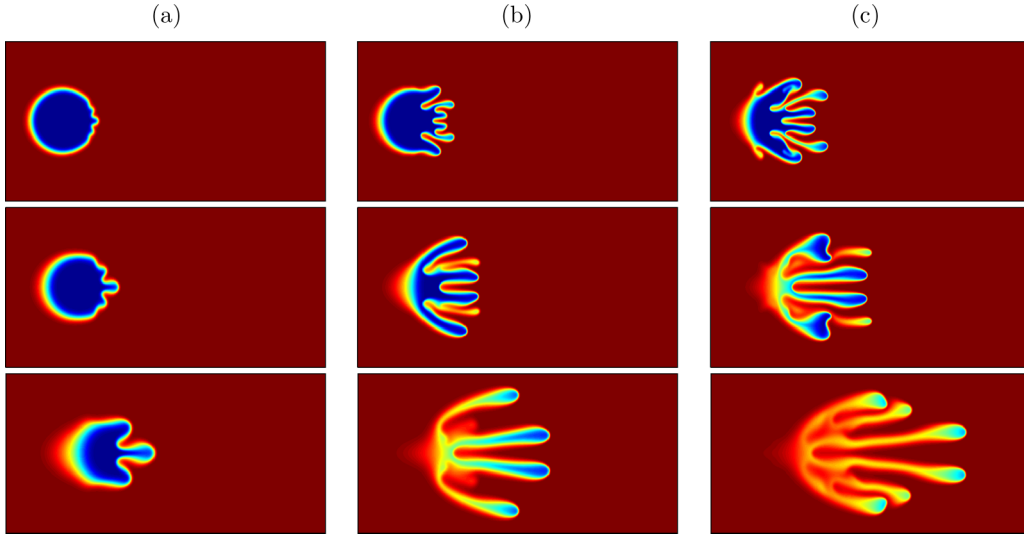


FIG. 5. Spatial distribution of concentration at $t = 1, 2, 4$ from top to bottom for $Pe = 1000$, $r = 0.5$, $\epsilon = 1$, and $R =$ (a) -0.5 , (b) -1 , (c) -1.5 .

the log-mobility ratio increases. This is qualitatively similar to the displacement of a less viscous finite slice. Given a pressure gradient, the less viscous blob moves faster than the ambient fluid and hence the fluid upstream to the blob in its vicinity are attracted towards the center of the blob. This is readily evident from the streamline distribution in the vicinity of the blob shown in Fig. 6 for $R = -1.5$, $r = 0.5$, and $Pe = 1000$. To analyze further, we summarize the stability characteristics in the parameter space spanned by R and Pe .

The observed difference between the dynamics of a more and less viscous circular blob raises a very intriguing question: Does there exist any critical blob radius for VF in a less viscous circular blob? De Wit and Homay [20] observed ellipse deformation and no VF in a less viscous blob of sufficiently small size. On the other hand, Chen *et al.* [28] reported VF for a less viscous blob of a given radius. This signifies that VF in a less viscous circular blob depends on the initial size of the blob. Here we are interested in estimating the critical blob radius for VF in a less viscous circular blob. We are also interested in exploring the dynamics of a less viscous circular blob of radius smaller than the critical value. It is observed that, similar to a more viscous blob, the critical blob radius for VF depends on R and Pe , i.e., $r_c(R, Pe)$. A series of numerical simulations with different values of Pe , R , and r yield the following values: $r_c(-1, 10^3) \approx 0.1$ and $r_c(-2, 225) \approx 0.5$. The overall qualitative dependence of r_c on the two flow parameters, R and Pe , are as follows: r_c decreases as R (or Pe) increases for a fixed Pe (or R). This is consistent with the effect of R and Pe on the VF instability, which is enhanced with both these parameters. We summarize in Fig. 7 the stability scenarios of a less viscous circular blob of initial radius $r = 0.5$ in the R - Pe parameter space. For a given Pe we vary R with increment 0.25 and perform numerical simulations to obtain the spatiotemporal dynamics of the blob. This procedure is followed for different Pe with increment 75. From visual inspection of the incipient deformation of the blob, we approximate the boundary between two adjacent stability regions. Next, we vary R and Pe in the neighborhood of the approximated boundaries with smaller increments than earlier.

This iterative process is repeated until satisfactory results are obtained for the boundaries. The symbols (square and circle) correspond to some of the data points used to calculate the

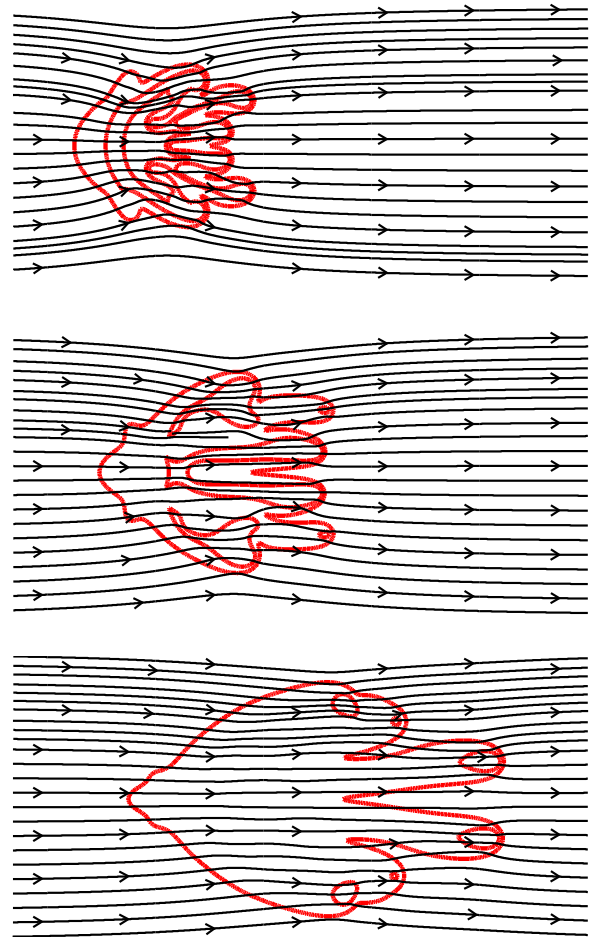


FIG. 6. Streamline distribution in the vicinity of a circular blob of radius $r = 0.5$ for $R = -1.5$ and $Pe = 1000$. From top to bottom: $t = 1, 2, 4$.

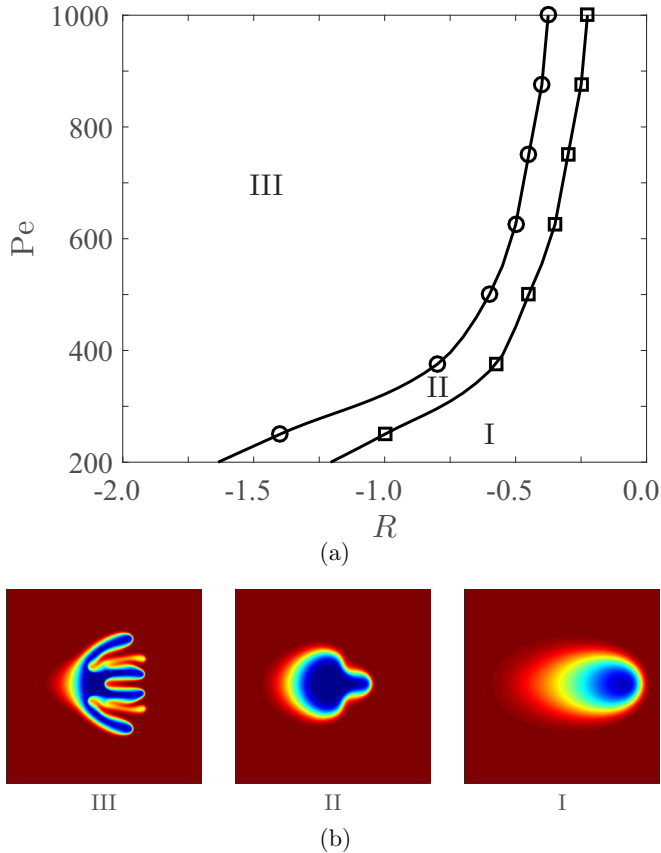


FIG. 7. (a) Phase plot in R - Pe plane for $r = 0.5$ shows three distinct instability regions: comet shaped (I), lump shaped (II), and VF (III). Region II corresponds to transition zone between the VF and comet-shaped instability. The symbols (\square or \circ) correspond to some of the data points used to calculate the boundaries between two adjacent stability regions. (b) Snapshots of the representative spatial structure of solute concentration c corresponding to each instability region are shown: VF ($R = -1$, $Pe = 10^3$), lump shaped ($R = -0.55$, $Pe = 625$), and comet shaped ($R = -0.35$, $Pe = 500$).

boundaries between two adjacent stability regions. Thus, we identify three instability regions: VF and comet- and lump-shaped deformation, similar to a more viscous circular blob. A noticeable difference between the instability regions of a more viscous blob and those of a less viscous one is best observed while moving along constant Pe lines in the parameter space. Along these lines, for $R < 0$, VF is observed for $R \leq R_c(r, Pe)$ and the instability becomes stronger as $|R|$ increases. As an example, for $r = 0.5$ and $Pe = 500$, the critical log-mobility ratio for VF is -0.6 , i.e., $R_c(0.5, 500) \approx -0.6$. This is in strong contrast with what happens for a more viscous blob that features VF only over a finite R window (see Fig. 4 of Pramanik *et al.* [32]). Another distinguished feature of a less viscous circular blob is that for a given blob radius r , and all finite Pe VF is observed for all $R < R_c(r, Pe)$. This is in stark contrast with the displacement of a more viscous blob, for which only comet-shaped deformation is observed below Pe_c [32].

The lump-shaped deformation, which, to the best of the authors' knowledge, was never discussed in the literature before, is one of the important results of the present study. Here we discuss the three instability modes and the underlying

physics. We move along the line $Pe = 500$ in the parameter space and successively choose $R = -0.35, -0.55$, and -1.50 , which correspond to the comet- and lump-shaped and VF instabilities, respectively. Figure 8(a) shows the spatiotemporal evolution of the solute concentration for $Pe = 500$, $R = -0.35$. The length of the curved diffusive interface with unstable viscosity contrast is too small to accommodate a single wavelength of the most unstable modes. Therefore, no VF is observed in this case.

Physical discussion of the development of the instability is best understood from a linear stability analysis. A linear stability analysis of the present problem is beyond the scope of this paper and will be addressed in our future research in a more general setting. However, the stability analysis of miscible rectilinear displacement at a planar interface [14,15,33] or radial source flow [34] reveals that the wave number of the unstable modes depends on time, in addition to other flow parameters (R , Pe). We know that the wavelength of the most unstable mode decreases as $|R|$ increases. This helps us to explain the possible origin of observed instabilities. For $R = -0.55$ the initial wavelength is smaller than the length of the unstable interface, such that part of the unstable interface tends to protrude as a finger. However, as time passes the wavelength of the unstable modes become too large to form fingering instability at the curved interface of the circular blob. Thus, the blob takes the shape of a comet after a long time. Therefore, we say that the parameter values of Fig. 8(b) and other similar values from region II on the parameter space corresponds to a transition from VF to comet-shaped deformation. For $R = -1.50$ the wavelength of the unstable mode becomes sufficiently small such that the curved miscible interface with unstable viscosity contrast contains more than one wave, which appears in the form of fingers.

Pramanik *et al.* [32] have shown that the dynamics of a more viscous blob depends not only on the curvature of the miscible interface of the blob but also on the distribution of the finite blob. In particular, the analysis of Pramanik *et al.* [32] suggests the existence of a finite R window for VF in a more viscous square blob in addition to a circular one (see Fig. 4 in Pramanik *et al.* [32]). This has been verified in this paper and is discussed in Sec. III B. A natural question follows: What is the influence of the flow of the ambient fluid around the blob on the spatiotemporal dynamics of a less viscous circular blob? This can be explained in terms of the velocity distribution in the neighborhood of the circular blob. Inside the blob the velocity is larger than that outside the blob. This results in the perturbations at the frontal interface of the circular blob that grow rapidly in the form of viscous fingers. We recall that the relative velocity between the circular blob and the ambient fluid increases with $|R|$, hence the instability becomes stronger (see Sec. III A). Similarly, the instability enhances when Pe increases, since larger Pe values correspond to higher flow rate for a given axial diffusion D_x (or small axial diffusion for a given flow rate, see Sec. III A). On the other hand, for a finite slice there is no passage for the displacing fluid to flow around the slice. In summary, the perturbations grow rapidly as the viscosity contrast increases irrespective of the shape of the less viscous finite sample and its extent allowing or hindering the flow of the ambient fluid past the finite sample. Thus, we conclude that, for a less viscous localized sample of different

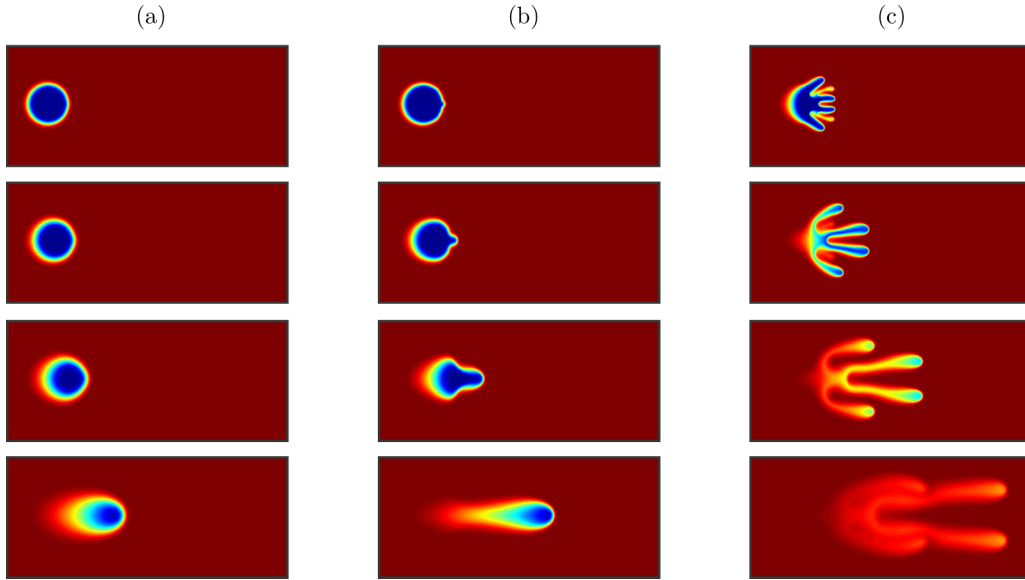


FIG. 8. Spatial distribution of the solute concentration at time $t = 1, 2, 4, 10$ (from top to bottom) for $r = 0.5$, $(Pe, R) =$ (a) $(500, -0.35)$, (b) $(625, -0.55)$, and (c) $(500, -1.5)$.

initial shape (circular and rectangular slice, for instance), the stability characteristics in the parameter plane spanned by R and Pe can be divided into two categories, VF and no VF. The no-VF region can be further subdivided into comet- and lump-shaped instabilities when the ambient fluid flows around the sample or only diffusive expansion of the miscible planar interface for a finite slice. The boundaries separating two adjacent stability regions depend on the flow parameters.

Next, we explore the influence of the blob radius on the observed dynamics while displacing a less viscous circular blob. We observe that the qualitative features of the different instability modes remain mostly unaffected by changing r . In particular, in Fig. 9 we show the influence of R and Pe on VF and comet- and lump-shaped instabilities for a less viscous circular blob of radius $r = 0.25$. This figure depicts that for $r = 0.25$ region III (corresponding to VF) shrinks, while regions I (comet-shaped deformation) and II (lump-shaped deformation) expand with respect to the corresponding regions for $r = 0.5$. One can easily derive similar R - Pe parameter space for different blob radius other than $r = 0.5$ (i.e., $r >, =, < 0.5$). For all r , three instability regions, mentioned in our results, will be observed apart from the quantitative changes. However, in the present paper the numerical simulations are performed for $r \leq 0.5$, due to the constraints of the numerical method (see Sec. IID).

IV. PARAMETRIC STUDY OF QUALITATIVE AND QUANTITATIVE PROPERTIES OF THE FLOW

In order to investigate the spreading of the blob we calculate the variance [18,32],

$$\sigma_x^2(t) = \frac{\int_0^{L_x} x^2 \bar{c}(x,t) dx}{\int_0^{L_x} \bar{c}(x,t) dx} - \left[\frac{\int_0^{L_x} x \bar{c}(x,t) dx}{\int_0^{L_x} \bar{c}(x,t) dx} \right]^2, \quad (11)$$

of the transversely averaged solute concentration, $\bar{c}(x,t) = \frac{1}{L_y} \int_0^{L_y} c(x,y,t) dy$, for different R and Pe . For a more viscous

circular blob, Pramanik *et al.* [32] showed that the tailing phenomenon enhances the spreading of the blob in the flow direction. We compare the longitudinal spreading of a circular blob when the viscosity of the blob is equal to ($R = 0$) and more ($R > 0$) and less ($R < 0$) than that of the ambient fluid. Figure 10 shows the temporal evolution of the axial variance of the transversely averaged solute concentration for $Pe = 1000$, $r = 0.5$ with $R = -0.5, 0$, and 0.5 . We show that the spreading of the circular blob in the flow direction increases as the viscosity contrast between the blob and ambient fluid increases. Initially, due to VF, a less viscous blob spreads more than a more viscous one. However, at later times the tailing

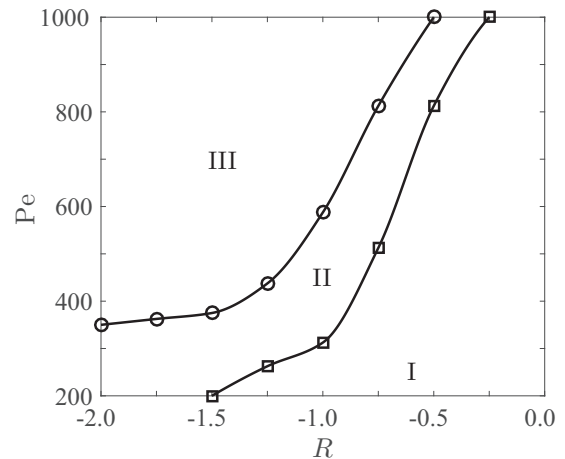


FIG. 9. Phase plot in the R - Pe plane for $r = 0.25$ shows three distinct instability regions: comet shaped (I), lump shaped (II), and VF (III), similar to the case of $r = 0.5$. The qualitative features remain unchanged by changing the blob radius. Quantitative behaviors of the three regions change: for decreasing r , region III shrinks, while regions I and II expand. The symbols (\square or \circ) correspond to some of the data points used to calculate the boundaries between two adjacent stability regions.

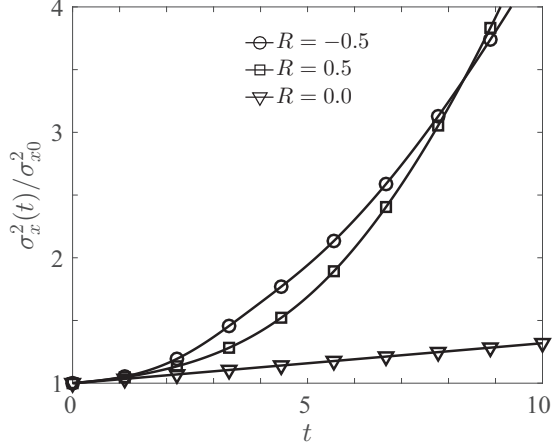


FIG. 10. Temporal evolution of the axial spreading relative to the initial extent, $\sigma_x^2(t)/\sigma_{x0}^2$, for $Pe = 1000$, $r = 0.5$.

phenomenon of the more viscous blob spreads the blob more along the flow direction than its less viscous counterpart.

In Sec. III A we showed that the flow of the displacing fluid around the miscible blob generates a tail in the downstream of a more viscous circular blob. On the other hand, for a less viscous blob VF is observed at the frontal curved interface of the blob. The influence of these phenomena on the spreading of the miscible blob differ completely. Here, we are interested in characterizing the spreading of a more or less viscous blob in the transverse direction in terms of the variance,

$$\sigma_y^2(t) = \frac{\int_0^{L_y} y^2 \bar{c}(y,t) dy}{\int_0^{L_y} \bar{c}(y,t) dy} - \left[\frac{\int_0^{L_y} y \bar{c}(y,t) dy}{\int_0^{L_y} \bar{c}(y,t) dy} \right]^2, \quad (12)$$

of the longitudinally averaged concentration profile, $\bar{c}(y,t) = \frac{1}{L_x} \int_0^{L_x} c(x,y,t) dx$. Temporal evolution of the transverse spreading of the circular blob relative to its initial extent in this direction, $\sigma_y^2(t)/\sigma_{y0}^2$, is presented in Fig. 11. Here, σ_{y0}^2 corresponds to the initial spreading of the circular blob in the transverse direction, i.e., $\sigma_y^2(t=0)$. It is observed that

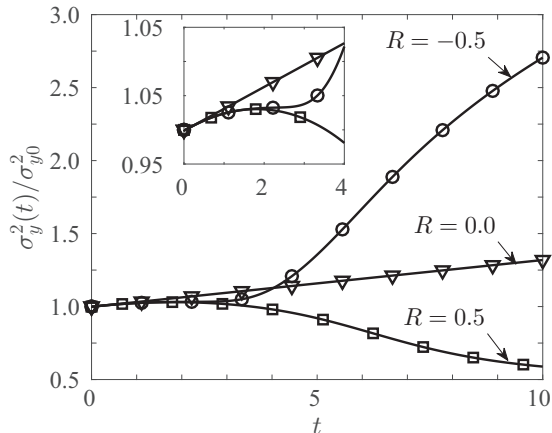


FIG. 11. Temporal evolution of the transverse spreading relative to the initial extent, $\sigma_y^2(t)/\sigma_{y0}^2$, for $Pe = 1000$, $r = 0.5$. Inset: At time $t \lesssim 4$, the transverse spreading for $R = 0$ is more than the corresponding values of $R \neq 0$.

at time $t \lesssim 4$, σ_y^2/σ_{y0}^2 is larger for $R = 0$ than $R \neq 0$. At later times, the magnitude of σ_y^2 depends on the sign of the log-mobility ratio R . For $R = -0.5$, VF is featured at the frontal part of the curved interface that increases $\sigma_y^2(t)$. On the other hand, for $R = 0.5$ comet-shaped deformation hinders the spreading in the transverse direction. Moreover, the more mobile ambient fluid sweeps away the transverse diffused layer in the downstream direction. Thus, a more viscous blob is narrowed in the transverse direction and this is characterized from $\sigma_y^2(t) < \sigma_{y0}^2$ (see Fig. 11).

Individually, the longitudinal or the transverse variance of the blob does not give the overall picture of the spreading and mixing of the blob in the ambient fluid. To have an estimate in this direction, we measure the area covered by the miscible blob

$$A(t) = \iint_{\Omega(t)} dx dy, \quad (13)$$

where $\Omega(t)$ is defined as, $\Omega(t) = \{(x,y) : 0.01 \leq c(x,y;t) \leq 0.99\}$, and $A_0 = A(t=0)$. The temporal evolution of the area of the miscible blob is shown in Fig. 12(a) for the parameter values of Fig. 11. It is observed that the less viscous circular blob spreads over the largest area than the more viscous and viscosity-matched blobs. For the parameter values used here, VF at the frontal curved interface of the less viscous blob increases the fluid-fluid interface and hence increases the area larger than the more viscous blob, which spreads only due to tail formation. The fluid mixing enhances due to diffusive mixing through the fluid-fluid interface. To quantify the mixing of the circular blob with the ambient fluid, we calculate the degree of mixing [1], $\chi(t) = 1 - \sigma^2(t)/\sigma_{\max}^2$, measured from the variance $\sigma^2(t) \equiv \langle c^2 \rangle - \langle c \rangle^2$ of the solute concentration. The temporal evolution of the degree of mixing for the parameter values of Fig. 12(a) are shown in Fig. 12(b). It is shown that the viscosity-matched blob mixes at a slower rate than a circular blob with viscosity mismatch. For $R = -0.5$ mixing is more than that for $R = 0.5$, since VF increases the fluid-fluid interface in the former than the latter.

A. Effect of anisotropic dispersion

In this section we explore the influence of dispersion anisotropy on the mixing of the blob in the ambient fluid. Figure 13(a) shows that, for a more viscous blob ($R > 0$), the mixing increases as ϵ approaches to ≈ 0.8 , and beyond this limit mixing reduces. Transverse dispersion and hence the diffusive mixing decreases as ϵ decreases. On the other hand, fingering instability becomes stronger and fine-scale structures are observed as ϵ decreases. Thus, the fluid-fluid interface, and hence the degree of mixing, increase. Here we discuss the effect of ϵ on the mixing of the circular blob at some time, say, $t = 10$. For $\epsilon \lesssim 0.8$ mixing due to dispersion dominates the mixing due to VF, thus resulting an overall increase in $\chi(t)$ as ϵ increases from 0.2 to 0.8. Beyond $\epsilon = 0.8$ the opposite phenomenon occurs. Thus, the result of these two opposite actions on the mixing of the blob is a nonmonotonic dependence of $\chi(t)$ on the anisotropic dispersion ϵ [see inset of Fig. 13(a)]. For $R < 0$, the diffusive mixing is smaller than the fingering mixing. This results a monotonic increment in $\chi(t)$ as ϵ increases [see inset of Fig. 13(b)].

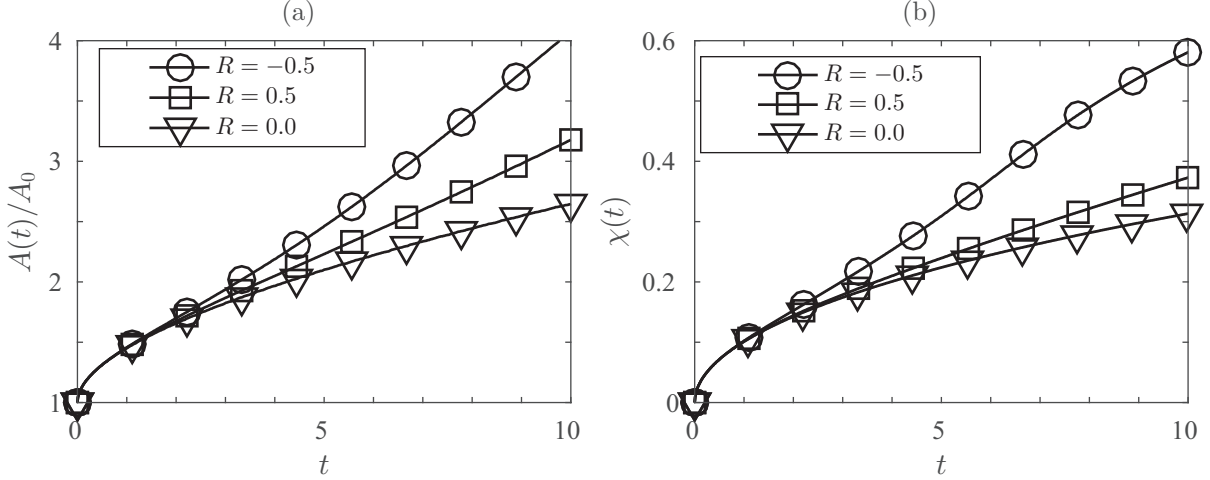


FIG. 12. For $Pe = 1000$ and different values of R , the temporal evolution of the (a) normalized area $A(t)/A_0$ occupied by the blob fluid and (b) degree of mixing $\chi(t)$ of a circular blob of radius $r = 0.5$.

V. BUOYANCY-DRIVEN FINGERING INSTABILITY IN VISCOSITY-MATCHED FLUIDS

Although the driving forces for VF and DF differ, the qualitative features of the instability and the finger patterns are similar [35]. Moreover, under certain conditions there exists a vertical flow equivalent to a horizontal flow [17]. This motivates us to investigate whether the convection-induced instability in a circular blob is equivalent to the instability originating from fluid displacement in viscosity-matched fluids. In this section we discuss the Rayleigh-Taylor instability at the upper or lower interface of a circular blob in a quiescent ambient fluid, when the dynamic viscosity of the two fluids are equal. This flow can be represented by the following nonlinear partial differential equations:

$$\nabla \cdot \underline{u} = 0, \quad \nabla p = -\underline{u} + \rho(c)\underline{i}, \quad (14)$$

$$\frac{\partial c}{\partial t} + \underline{u} \cdot \nabla c = \frac{\nabla^2 c}{Ra}, \quad (15)$$

in dimensionless form. Here p is the hydrostatic pressure head. There is no applied pressure gradient that can originate flow

in the system. For dimensionless formulation we use the same characteristic scales as in Sec. II B, except $V_c = |\Delta\rho|\kappa g/\mu$, the buoyancy-induced convective velocity. Here $\Delta\rho = \rho_2 - \rho_1$ represents the difference between the density of the two fluids, g is the magnitude of the gravitational acceleration, μ is the dynamic viscosity of the fluid, and the density of the fluids is given by

$$\rho(c) = \begin{cases} c, & \text{if } \rho_2 > \rho_1 \\ 1 - c, & \text{if } \rho_2 < \rho_1 \end{cases} \quad (16)$$

We numerically solve this problem using the method discussed in Sec. II D to analyze the dynamics of a heavy or light blob in a quiescent fluid. Thus, Eqs. (14) and (15) are recast in terms of the stream function as

$$\nabla^2 \psi = \frac{\partial \rho}{\partial c} \frac{\partial c}{\partial y}, \quad (17)$$

$$\frac{\partial c}{\partial t} + \frac{\partial \psi}{\partial y} \frac{\partial c}{\partial x} - \frac{\partial \psi}{\partial x} \frac{\partial c}{\partial y} = \frac{\nabla^2 c}{Ra}, \quad (18)$$

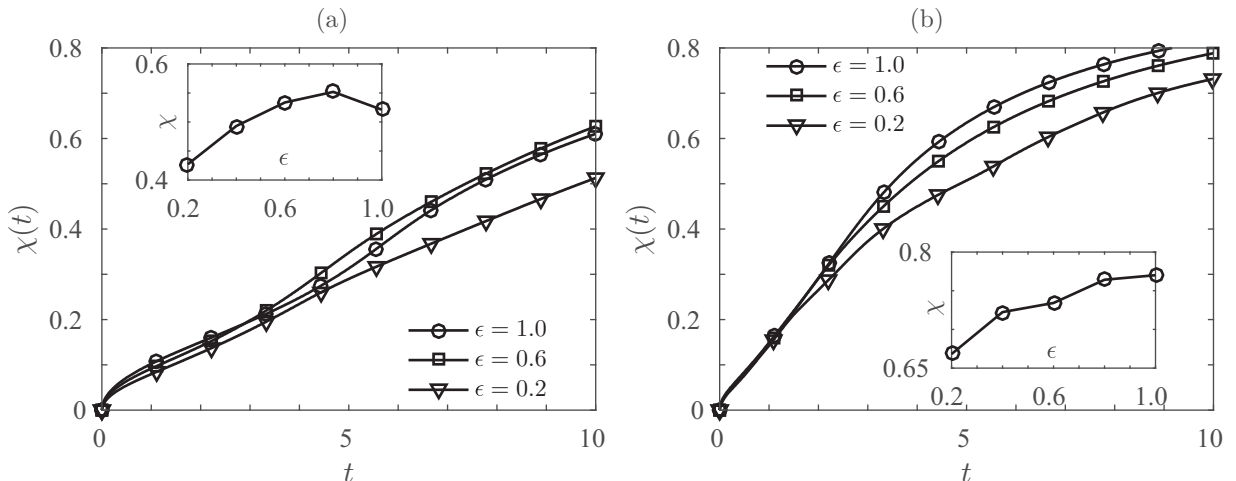


FIG. 13. Effect of anisotropic dispersion on the degree of mixing, $\chi(t)$, for $r = 0.5$, $Pe = 1000$, (a) $R = 1$, (b) $R = -1$. Inset: Variation of χ with ϵ at time $t = 8$.

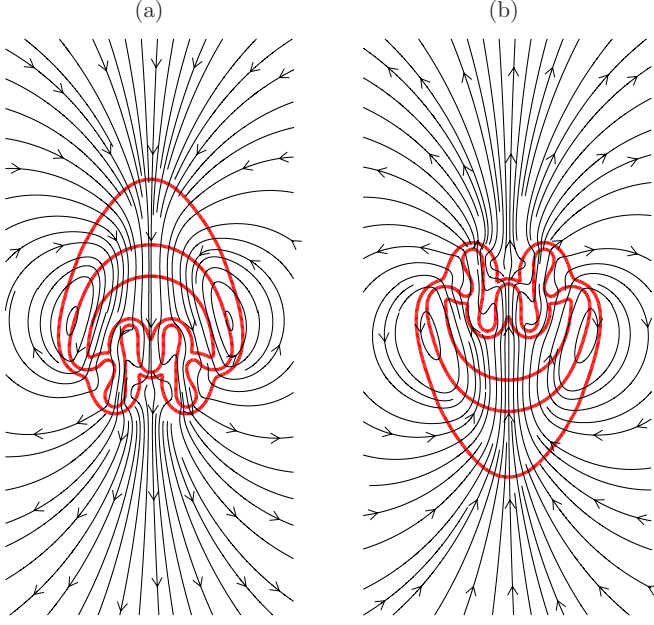


FIG. 14. Streamlines in the vicinity of the blob for $Ra = 1000$, and (a) $\rho_1 < \rho_2$, (b) $\rho_1 > \rho_2$. The blob is represented by isocontours of solute concentration c (red). The contour values are $c = 0.01, 0.5, 0.99$ (from outside to inside).

where $Ra = V_c L_c / D$ is the solutal Rayleigh number, and D is the constant isotropic dispersion coefficient of the solute.

Figures 14(a) and 14(b) show the streamlines distribution in the vicinity of a heavy and light blob, respectively. These

figures show that the density-driven instability at the lower interface (heavier blob) is identical to that at the upper interface (lighter blob). In the former the heavier blob acquires a downward movement under the action of gravitational acceleration, while the lighter blob, in the latter case, climbs upward against the gravitational force. Due to the movement of the blob, circulations are generated on the two lateral sides of the blob, which helps in fluid mixing. This is readily observed from the streamlines distribution in the vicinity of the blob.

Here we present a simple mathematical analysis to explain the observed dynamics of a heavy or light blob. When the density of the blob is less than the ambient fluid, we take the coordinate transformation, $X = L_x - x, Y = L_y - y$, where L_x and L_y are the dimensionless length and width of the domain. Therefore, we have

$$\frac{d^n}{dx^n} = (-1)^n \frac{d^n}{dX^n}, \quad \frac{d^n}{dy^n} = (-1)^n \frac{d^n}{dY^n}, \quad \forall n \in \mathbb{N}. \quad (19)$$

Therefore, the equations of motion in this transformed coordinate system are (gravity working in the negative X direction)

$$\tilde{\nabla} \cdot \tilde{\mathbf{u}} = 0, \quad \tilde{\nabla} p = -\tilde{\mathbf{u}} - \rho(c)\hat{\mathbf{i}}, \quad (20)$$

$$\frac{\partial c}{\partial t} + \tilde{\mathbf{u}} \cdot \tilde{\nabla} c = \frac{\tilde{\nabla}^2 c}{Ra}, \quad (21)$$

where $\tilde{\mathbf{u}}$ is the Darcy velocity in (X, Y) coordinates and $\tilde{\nabla} = (\frac{\partial}{\partial X}, \frac{\partial}{\partial Y})$. Darcy's law in Eq. (20) can be written in component form as

$$\begin{aligned} \frac{\partial p}{\partial X} &= -\tilde{u} - \rho(c), & \frac{\partial p}{\partial Y} &= -\tilde{v}, \\ \text{or, } -\frac{\partial p}{\partial x} &= -\tilde{u} - \rho(c), & -\frac{\partial p}{\partial y} &= -\tilde{v}, \quad [\text{from Eq. (19)}] \\ \text{or, } -(-u + \rho(c)) &= -\tilde{u} - \rho(c), & -(-v) &= -\tilde{v}, \quad [\text{from Eq. (14)}] \\ \text{or, } u - \rho(c) &= -\tilde{u} - \rho(c), & v &= -\tilde{v}, \\ \text{or, } u = -\tilde{u}, & v = -\tilde{v}, & \text{i.e., } \underline{\mathbf{u}} &= -\tilde{\underline{\mathbf{u}}}. \end{aligned} \quad (22)$$

Again, the convection diffusion equation (21) gives

$$\begin{aligned} \frac{\partial c}{\partial t} + \tilde{u} \frac{\partial c}{\partial X} + \tilde{v} \frac{\partial c}{\partial Y} &= \frac{1}{Ra} \left(\frac{\partial^2 c}{\partial X^2} + \frac{\partial^2 c}{\partial Y^2} \right), \\ \text{or, } \frac{\partial c}{\partial t} + (-u) \left(-\frac{\partial c}{\partial x} \right) + (-v) \left(-\frac{\partial c}{\partial y} \right) &= \frac{1}{Ra} \left(\frac{\partial^2 c}{\partial x^2} + \frac{\partial^2 c}{\partial y^2} \right), \quad [\text{from Eqs. (19) and (22)}] \\ \text{or, } \frac{\partial c}{\partial t} + u \frac{\partial c}{\partial x} + v \frac{\partial c}{\partial y} &= \frac{1}{Ra} \left(\frac{\partial^2 c}{\partial x^2} + \frac{\partial^2 c}{\partial y^2} \right), \end{aligned} \quad (23)$$

which is the same as Eq. (15). Equations (22) and (23) show that in the two cases of heavy and light blobs, the velocity are of equal magnitude in opposite directions, and the dynamics of the solute concentration is governed by the same equation. Therefore, we conclude that the fingering dynamics of a heavy blob is a mirror image to that of a light blob, as captured from the numerical simulations.

VI. CONCLUSION

We investigate the deformation of a more or less viscous sample (circular or square) displaced by a fluid of different viscosity. The stability scenarios are summarized in the parameter space spanned by R and Pe . For an initially circular blob, three instability modes are observed for both $R > 0$ and $R < 0$. The most striking difference between a more and a

less viscous circular sample is the finite R window for VF. In the latter case there does not exist any such R window for VF. For a less viscous blob, beyond the critical value of the log-mobility ratio, VF enhances with the magnitude of R . This qualitative property of the instability in a less viscous circular blob is similar to that of a less viscous finite slice. The critical blob radius for VF is smaller for $R < 0$ than its $R > 0$ counterpart. It is observed that the mixing of a less viscous blob with the ambient fluid increases with the viscosity contrast, while the mixing of a more viscous circular blob depends nonmonotonically on R . Furthermore, the degree of mixing of more viscous blob has nonmonotonic dependence on the dispersion anisotropy, while, for a less viscous blob, mixing increases monotonically as ϵ decreases.

We further analyze the instability in the rectilinear displacement of an initially square blob. It is shown that for a more viscous blob the lump-shaped instability mode disappears. Moreover, in the case of a square blob, the VF region is larger than that for a circular blob which inscribes the square blob. The critical Péclet number, Pe_c , for VF is smaller for a square blob than the corresponding circular blob. However, the critical log-mobility ratio, R_c , remains almost the same for both the circular and the corresponding square blob. When the

viscosity of the square sample is less than the displacing fluid, there exist two instability modes similar to its more viscous counterpart. The region of VF is larger for a less viscous square sample compared to the corresponding circular one. Finally, we have shown that the Rayleigh-Taylor instability in a circular blob in a quiescent fluid is independent of the curvature of the unstable interface, which completely differs from its VF counterpart. We believe our finding will motivate more theoretical and experimental studies in the context of hydrodynamic instabilities in porous media. Moreover, the effect of shear stress on these types of instabilities would be more interesting to the fluid dynamists and physicists.

ACKNOWLEDGMENTS

S.P. is thankful to the National Board for Higher Mathematics (NBHM), Department of Atomic Energy (DAE), Government of India for financial support [sanction order no. 2/39(15)/2011/R&D-II/8839]. The authors are grateful to A. De Wit (ULB, Brussels) for fruitful discussion. S.P. is grateful to Vandita Sharma for helping with some of the numerical computations.

-
- [1] B. Jha, L. Cueto-Felgueroso, and R. Juanes, Fluid Mixing from Viscous Fingering, *Phys. Rev. Lett.* **106**, 194502 (2011).
 - [2] B. Jha, L. Cueto-Felgueroso, and R. Juanes, Synergetic Fluid Mixing from Viscous Fingering and Alternating Injection, *Phys. Rev. Lett.* **111**, 144501 (2013).
 - [3] G. M. Homsy, Viscous fingering in porous media, *Annu. Rev. Fluid Mech.* **19**, 271 (1987).
 - [4] C. Welty, A. C. Kane III, and L. J. Kauffman, Stochastic analysis of transverse dispersion in density-coupled transport in aquifers, *Water Resour. Res.* **39**, 1150 (2003).
 - [5] H. E. Huppert and J. A. Neufeld, The fluid mechanics of carbon dioxide sequestration, *Annu. Rev. Fluid Mech.* **46**, 255 (2014).
 - [6] V. Lagneau, A. Pipart, and H. Catalette, Reactive transport modeling of CO₂ sequestration in deep saline aquifers, *Oil Gas Sci. Technol. Rev. IFP* **60**, 231 (2005).
 - [7] M. Sauzade and T. Cubaud, Initial microfluidic dissolution regime of CO₂ bubbles in viscous oils, *Phys. Rev. E* **88**, 051001(R) (2013).
 - [8] A. De Wit, Y. Bertho, and M. Martin, Viscous fingering of miscible slices, *Phys. Fluids* **17**, 054114 (2005).
 - [9] C. Rana, M. Martin, A. De Wit, and M. Mishra, Combined influences of viscous fingering and solvent effect on the distribution of adsorbed solutes in porous media, *RSC Adv.* **4**, 34369 (2014).
 - [10] C. Rana and M. Mishra, Fingering dynamics on the adsorbed solute with influence of less viscous and strong sample solvent, *J. Chem. Phys.* **141**, 214701 (2014).
 - [11] A. Riaz, M. Hesse, H. A. Tchelepi, and F. M. Orr, Jr., Onset of convection in a gravitationally unstable diffusive boundary layer in porous media, *J. Fluid Mech.* **548**, 87 (2006).
 - [12] M. Mishra, A. De Wit, and K. C. Sahu, Double diffusive effects on pressure-driven miscible displacement flows in a channel, *J. Fluid Mech.* **712**, 579 (2012).
 - [13] R. Govindarajan and K. C. Sahu, Instabilities in viscosity-stratified flow, *Annu. Rev. Fluid Mech.* **46**, 331 (2014).
 - [14] C. T. Tan and G. M. Homsy, Stability of miscible displacements in porous media: Rectilinear flow, *Phys. Fluids* **29**, 3549 (1996).
 - [15] C. T. Tan and G. M. Homsy, Simulation of non-linear viscous fingering in miscible displacement, *Phys. Fluids* **31**, 1330 (1988).
 - [16] V. Loodts, C. Thomas, L. Rongy, and A. De Wit, Control of Convective Dissolution by Chemical Reactions: General Classification and Application to CO₂ Dissolution in Reactive Aqueous Solutions, *Phys. Rev. Lett.* **113**, 114501 (2014).
 - [17] O. Manickam and G. M. Homsy, Fingering instabilities in vertical miscible displacement flow in porous media, *J. Fluid Mech.* **288**, 75 (1995).
 - [18] M. Mishra, M. Martin, and A. De Wit, Differences in miscible viscous fingering of finite width slices with positive or negative log mobility ratio, *Phys. Rev. E* **78**, 066306 (2008).
 - [19] M. Mishra, P. M. J. Trevelyan, C. Almarcha, and A. De Wit, Influence of Double Diffusive Effects on Miscible Viscous Fingering, *Phys. Rev. Lett.* **105**, 204501 (2010).
 - [20] A. De Wit and G. M. Homsy, Viscous fingering in reaction-diffusion systems, *J. Chem. Phys.* **110**, 8663 (1999).
 - [21] C. Nicolaidis, B. Jha, L. Cueto-Felgueroso, and R. Juanes, Impact of viscous fingering and permeability heterogeneity on fluid mixing in porous media, *Water Resour. Res.* **51**, 2634 (2015).
 - [22] J. R. Boulding, *EPA Environmental Assessment Sourcebook* (Ann Arbor Press, Chelsea, Mich., 1996), pp. 113–175.
 - [23] P. J. Cullen, *Food Mixing: Principles and Applications* (Wiley, New York, 2009).

- [24] P. Olson, P. G. Silver, and R. W. Carlson, The large-scale structure of convection in the Earth's mantle, *Nature (London)* **344**, 209 (1990).
- [25] J. Hatwalne, S. Ramaswamy, M. Rao, and R. A. Simha, Rheology of Active-Particle Suspensions, *Phys. Rev. Lett.* **92**, 118101 (2004).
- [26] H. Kurtuldu, J. S. Guasto, K. A. Johnson, and J. P. Gollub, Enhancement of biomixing by swimming algal cells in two-dimensional films, *Proc. Natl. Acad. Sci. USA* **108**, 10391 (2011).
- [27] M. Dentz, T. Le Borgne, A. Englert, and B. Bijeljic, Mixing, spreading and reaction in heterogeneous media: A brief review, *J. Contam. Hydrol.* **120-121**, 1 (2011).
- [28] C.-Y. Chen, L. Wang, and E. Meiburg, Miscible droplet in a porous medium and the effects of Korteweg stresses, *Phys. Fluids* **13**, 2447 (2001).
- [29] R. Maes, G. Rousseaux, B. Scheid, M. Mishra, P. Colinet, and A. De Wit, Experimental study of dispersion and miscible viscous fingering of initially circular sample in Hele-Shaw cells, *Phys. Fluids* **22**, 123104 (2010).
- [30] J. Mainhagu, F. Golfier, C. Oltéan, and M. A. Buès, Gravity-driven fingers in fractures: Experimental study and dispersion analysis by moment method for a point-source injection, *J. Contam. Hydrol.* **132**, 12 (2012).
- [31] M. Sajjadi and J. Azaiez, Heat and mass transfer in melting porous media: Stable miscible displacements, *Int. J. Heat Mass Transf.* **88**, 926 (2015).
- [32] S. Pramanik, A. De Wit, and M. Mishra, Viscous fingering and deformation of a miscible circular blob in a rectilinear displacement in porous media, *J. Fluid Mech. Rapids* **782**, R2 (2015).
- [33] S. Pramanik and M. Mishra, Effect of Péclet number on miscible rectilinear displacement in a Hele-Shaw cell, *Phys. Rev. E* **91**, 033006 (2015).
- [34] C. T. Tan and G. M. Homsy, Stability of miscible displacements in porous media: Radial source flow, *Phys. Fluids* **30**, 1239 (1987).
- [35] M. P. M. A. Baroni, A. De Wit, and R. R. Rosa, Detrended fluctuation analysis of numerical density and viscous fingering patterns, *Europhys. Lett.* **92**, 64002 (2010).